# Supplementary Materials for

## Protein assemblies ejected directly from native membranes yield intact complexes for mass spectrometry

Dror S. Chorev[1], Lindsay A. Baker[2], Di Wu[1], Victoria Beilsten-Edmands[1], Sarah L. Rouse[3], Tzviya Zeev-Ben-Mordehai[2,#], Chimari Jiko[4], Firdaus Samsudin[5], Christoph Gerle[6,7], Syma Khalid[5], Alastair G. Stewart[8,9], Stephen J. Matthews[3], Kay Grünewald[2,10], and Carol V. Robinson[1,*].

Correspondence to: carol.robinson@chem.ox.ac.uk

**This PDF file includes:**

## Materials and Methods

### Outer and Inner Membrane Vesicle Preparation

Outer and inner membranes were prepared as described previously (*41*). Briefly, 0.5 L *E. coli* BL21 was grown in LB to OD 2.0 at 37 °C with 250 rpm shaking, before harvesting the cells by centrifugation at 4000xg for 10 min. Cells were resuspended in buffer A (50 mM Tris pH 7.4, 150 mM NaCl) and lysed with a constant flow cell disruptor at 8-12 kpsi. Cell debris was removed by centrifugation at 4000xg for 10 min, and membranes were harvested by ultracentrifugation in a Beckman SW32Ti rotor for 1 hour at 25000 rpm. The supernatant was removed and the membranes were resuspended in 5.8 mL of buffer A with 20% sucrose, before layering on a discrete sucrose gradient in buffer A (0.85 mL 55% sucrose, 11.4 mL 51% sucrose, 11.4 mL 45% sucrose, 7.8 mL 36% sucrose) and centrifuging for 17 h at 30000 rpm in a SW32Ti rotor. Outer and inner membranes were removed from the interface of the 55% and 51% and 45% and 36% sucrose layers respectively and washed twice in ~38 mL lysis buffer without sucrose by centrifuging at 25000 rpm for 1 hr in a SW32Ti. Membranes were then resuspended in 0.5-1 mL buffer A and stored at 4°C until further use.

### MPEEV Preparation

BHK-21 cells were grown in Glasgow MEM containing 10% FBS, 20 mM HEPES and 2% Triptose Phosphate Broth at 37 °C, 5% $CO_2$ 24 h before transfection, $15x10^6$ cells were seeded onto a T175 cell culture flask. Cells were transfected using 60 µg of selected DNA utilizing Lipofectamine 2000 according to the manufacturer's protocol. 2 h post transfections, cells were washed with PBS and media was changed with 2% FBS in GMEM. 24 h after transfection cells were washed and medium was replaced with serum free GMEM. 2 days following transfection, medium was collected and centrifuged at 30,000 rpm in a Beckman ultracentrifuge utilizing an SW32Ti rotor. The supernatant was then removed and vesicles were resolubilized in 500 mM Ammonium Acetate at pH 7.6.

### Preparation of mitochondrial membranes

Mitochondrial inner membranes were prepared as previously described (*42*). In brief, after careful removal of fat and connective tissues, bovine heart muscle of one fresh bovine heart was minced using a commercial meat mincer. A 600 g portion of minced meat was suspended on ice in 2,650 mL of 26 mM sodium phosphate buffer, pH 7.4, and homogenized for 10 min at 11,000 rpm in a Polytron PT3100D homogenizer, followed by centrifugation for 20 min at 2,800 rpm in a large-

scale refrigerated centrifuge (Hitachi himac CR20G) using an R9A rotor at 4 °C. All supernatants were combined and centrifuged for 25 min at 4 °C and 8,000 rpm in a Hitachi Himac CR20G centrifuge using a R12AF rotor. The precipitate, suspended in 40 mM HEPES buffer (pH 7.8), 0.5mM EGTA/EDTA and 1mM DTT, was centrifuged for 30 min at 30,000 rpm in a P45AT rotor using a Hitachi Himac CP80WX ultracentrifuge. Finally, the precipitate was suspended in 40 mM HEPES buffer (pH 7.8), 2 mM $MgCl_2$, 0.5 mM EGTA/EDTA, 1 mM DTT, and the protein concentration adjusted to 26.8 mg/ml.

For outer and inner membrane preparations that were not separated, membranes were prepared in the same way but without the osmotic bursting and ultra-centrifugation steps.

**Sonication of Membranes for Native Mass Spectrometry**

Collected vesicles were diluted in 20 ml of 500 mM Ammonium acetate, and sonicated using a probe sonicator (Vibra-Cell VCX-500 Watt, Sonics) using maximal amplitude. Volume was then reduced to ~200 microliters using a 10-50 kDa cut-off concentrating tube (Milipore).

**Native Mass Spectrometry**

Native mass spectrometry experiments were carried out on a Q-Exactive Plus UHMR (*11*) modified to facilitate the transmission of high-energy species (*43*) and adapted for membrane proteins (*44*). The following parameters were used: Capillary Voltage - 1.6 kV, Dessolvation voltage- -200 V, Source fragmentation - 200 V, HCD energy - 0-300 V. HCD pressure was set to 6, the equivalent of $1.8x10^{-9}$ bar. EMR was set to on, C-trap entrance lens tune offset was set to 2, injection flatopole was set to 8 V, inter flatopole lens was at 6V, and bent flatopole at 4 V. Threshold was set to 3. Data was analysed using Xcalibur 2.2 (Thermo Fischer) and Masslynx 4.2 (Waters).

**Lipidomics**

MPEEVs in Ammonium Acetate were lyophilized by a vacuum concentrator (Savant SPD1010 SpeedVac Concentrator, Thermo Scientific). The lipid/protein mixture was then re-dissolved in 60% acetonitrile (ACN) by sonication for 10 min. For LC-MS/MS analysis, the lipids were separated on a C18 column (Acclaim PepMap 100, C18, 75 µm × 15 cm; Thermo Scientific) by Dionex UltiMate 3000 RSLC nano System connected to a hybrid LTQ Orbitrap mass spectrometer (Thermo Scientific) via a dynamic nanospray source. The buffers and gradient are adapted from (*45*). Briefly, a binary buffer system was used with buffer A of ACN: $H_2O$ (60:40), 10 mM

ammonium formate, 0.1% formic acid and buffer B of IPA: ACN (90:10), 10 mM ammonium formate, 0.1% formic acid. The phospholipids were separated at 40 °C with a gradient of 32% to 99% buffer B at a flow rate of 300 nl/min over 30 min. Typical MS conditions were a spray voltage of 1.8 kV and capillary temperature of 175 °C. The LTQ-Orbitrap XL was operated in negative ion mode and in data-dependent acquisition with one MS scan followed by five MS/MS scans. Survey full-scan spectra were acquired in the orbitrap (m/z 350 − 2,000) with a resolution of 60,000. Collision-induced dissociation (CID) fragmentation in the linear ion trap was performed for the five most intense ions at an automatic gain control target of 30,000 and a normalized collision energy of 38% at an activation of q = 0.25 and an activation time of 30 ms (*45*, *46*).

**Protein identification and proteomics**

For identification of proteins, protein bands were excised from the gel and processed as described (*47*). Peptides were re-suspended in 0.1% Formic Acid and separated on an Ultimate 3000 UHPLC system (Thermo Fisher Scientific) and electrosprayed directly into a Q Exactive mass spectrometer (Thermo Fisher Scientific) through an EASY-Spray nano-electrospray ion source (Thermo Fisher Scientific). The peptides were trapped on a C18 PepMap100 pre-column (300 µm i.d. x 5 mm, 100 Å, Thermo Fisher Scientific) using solvent A (0.1% Formic Acid in water) at a pressure of 500 bar. The peptides were separated on an analytical column (75 µm i.d. packed in-house with ReproSil-Pur 120 C18-AQ, 1.9 µm, 120 Å, Dr Maisch GmbH) using a gradient (15% to 38% for 30 min, solvent B - 0.1% formic acid in acetonitrile, flow rate: 200 nL/min) for 15 min. The raw data was acquired in a data-dependent acquisition mode (DDA). Full scan mass spectra were acquired in the Orbitrap (scan range 350-1500 m/z, resolution 70000, AGC target 3e6, maximum injection time 50 ms). After the MS scans, the 10 most intense peaks were selected for HCD fragmentation at 30% of the normalized collision energy. HCD spectra were also acquired in the Orbitrap (resolution 17500, AGC target 5e4, maximum injection time 120 ms) with first fixed mass at 180 m/z. Charge exclusion was selected for 1+ and 2+ ions. The dynamic exclusion set to 5 secs. All peptides were manually validated. Peptide identification was done using the MASCOT Daemon client program.

**Electron cryo-microscopy**

Inner and outer membranes were applied to Quantifoil 2/1 holey carbon grids after glow-discharging for 1 min 30 s on high (30 W) in a PDC-002-CE Plasma Cleaner (Harrick Plasma Ithaca, United States), before blotting for 8 s by hand and plunging into a bath of propane/ethane

with a manual plunger. Grids were stored under liquid nitrogen until imaging. EM data was recorded on either a TF30 or TF30 Polara (ThermoFisher/FEI), equipped with K2 direct electron detectors and Quantum energy filters (Gatan). Data was collected with SerialEM (*48*), with pixel sizes between 2 and 3 Å/pixel at the specimen level and the energy selecting slit set to 20 eV, as movies with 5 frames per second in counting mode at a dose rate of ~5$e^-$/unbinned pix/sec, giving an overall dose of ~ 10-20 $e^-/Å^2$ on the sample. Frames were aligned and averaged in SerialEM.

**Molecular Dynamics Simulations**

For the Bam complex, the model outer membrane was constructed using the CHARMM-GUI web server (*49*) based on the lipid composition of *E. coli* K12 (100% Re LPS in the upper leaflet; 90% POPE, 5% POPG and 5% cardiolipin in the lower leaflet (*49*). The structure of the $BamABCD(E)_2$ complex was generated by aligning the BamE dimer (PDB: 2YH9) (*50*) to the BamE subunit in the BamABCDE complex (PDB: 5D0O) (*16*) using PyMOL. The atomic structures of BamABCDE and $BamABCD(E)_2$ were converted to coarse-grained representations using MARTINI 2.2 force field with the ELNEDYN elastic network model utilized to maintain the secondary structure (*51*). These protein complexes were embedded into the membrane and overlapping lipids were removed. The standard MARTINI water molecules were added to solvate the system, while 170 mM $Ca^{2+}$ ions and 150 mM NaCl were used to neutralize the system. Energy minimization was performed following the steepest descent protocol. A short 10 ns equilibration simulation was conducted with position restraints imposed on the protein. These restraints were then removed and three independent 5 μs simulations (starting with different initial velocity distributions) were run for each system. The temperature was maintained at 323 K using the velocity rescaling thermostat (*52*) and the pressure was kept at 1 atm using the Parrinello-Rahman barostat (*53*). All simulations were performed using the GROMACS 2018 software.

For ANT1, simulations were performed using the gromacs 4.6.7 (www.gromacs.org) package (*54*) with GPU acceleration. Initial atomistic coordinates for the ADP/ATP translocase (ANT1) PDB id 1OKC (*35*) were taken from the MemProtMD database and Martini v2.2 coarse grained parameters were generated using the martinize.py script with an elastic network of 1 nm cutoff and a force constant of 500 kJ $mol^{-1}$ $nm^{-2}$. Two molecules of ANT1 were placed in the xy-plane 9 nm apart in a simulation box of 18 x 18 x 10 nm and POPC:POPE:CDL:PLM membranes were generated by self-assembly with the protein positionally restrained as described elsewhere. To achieve an asymmetric membrane CDL was added to one side only of the simulation box.

Production runs were 5 μs each. Simulations were performed at 310 K using the V-rescale algorithm (*52*) and 1 tau using the Parrinello-Rahman barostat with semiisotropic coupling. Visualisation used Pymol (http://pymol.org) and VMD (*55*). Lipid density isosurfaces of phosphate particles in the reference frame of the protein were generated using the Volmap plugin of VMD.

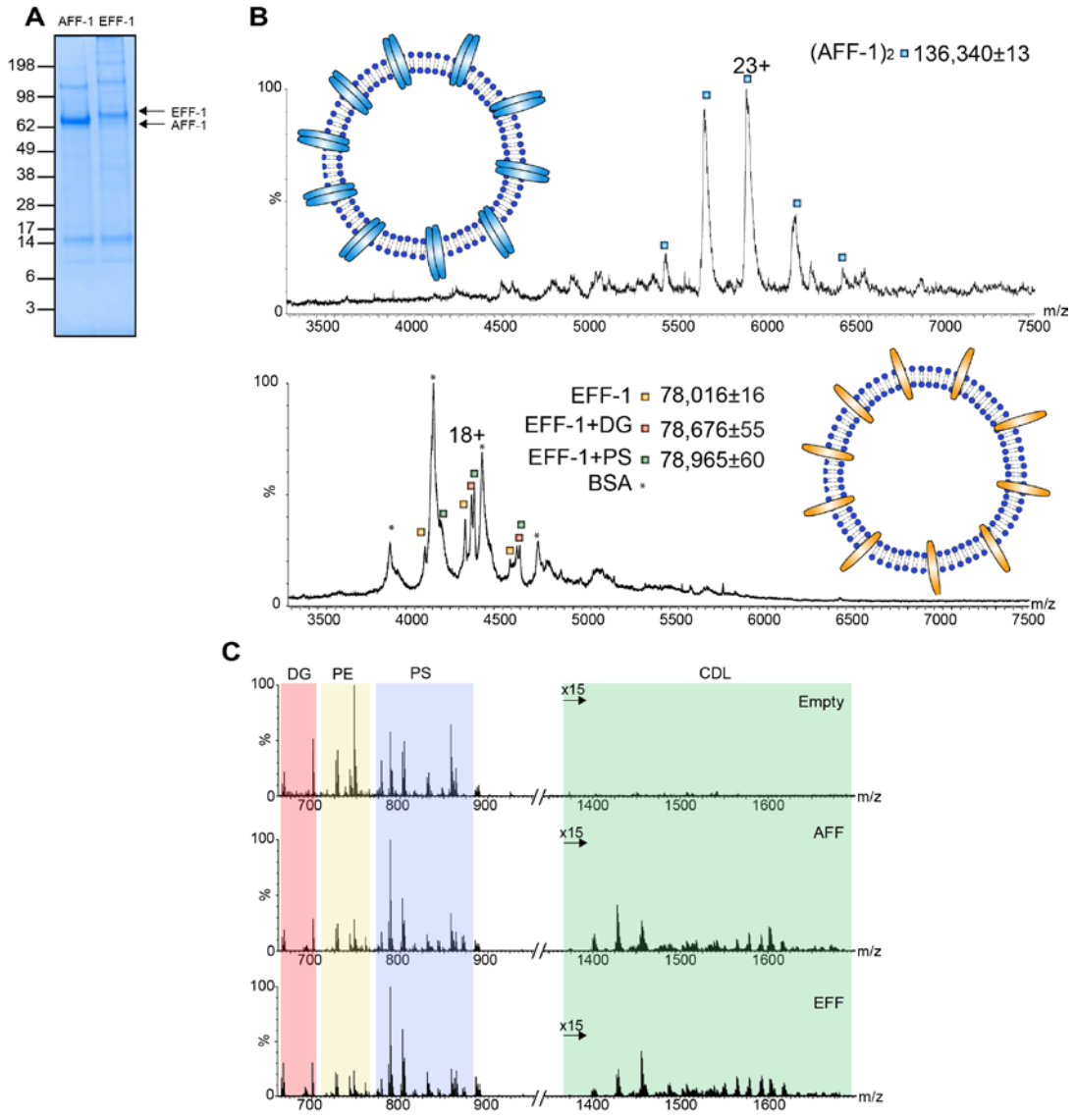


**Fig. S1. AFF-1 and EFF-1 ejected from membrane protein enriched extra cellular vesicles as a dimeric assembly and a lipid bound monomer. A** SDS-PAGE analysis of MPEEVs shows predominantly AFF-1 and EFF-1. **B** Predominant charge state series in the native mass spectrum of sonicated MPEEVs reveals dimeric AFF-1 and lipid bound monomeric EFF-1 with BSA carried over from cell growth serum. **C** Lipidomics comparison of empty and AFF-1 or EFF-1 containing vesicles reveals an increased levels of cardiolipin upon overexpression of the two proteins. Different lipids are highlighted as follows: DG- Diacylglycerol (pink), PE- phosphatydilethanolamine (yellow), PS- phosphatydilserine (blue), CDL- cardiolipin (green).

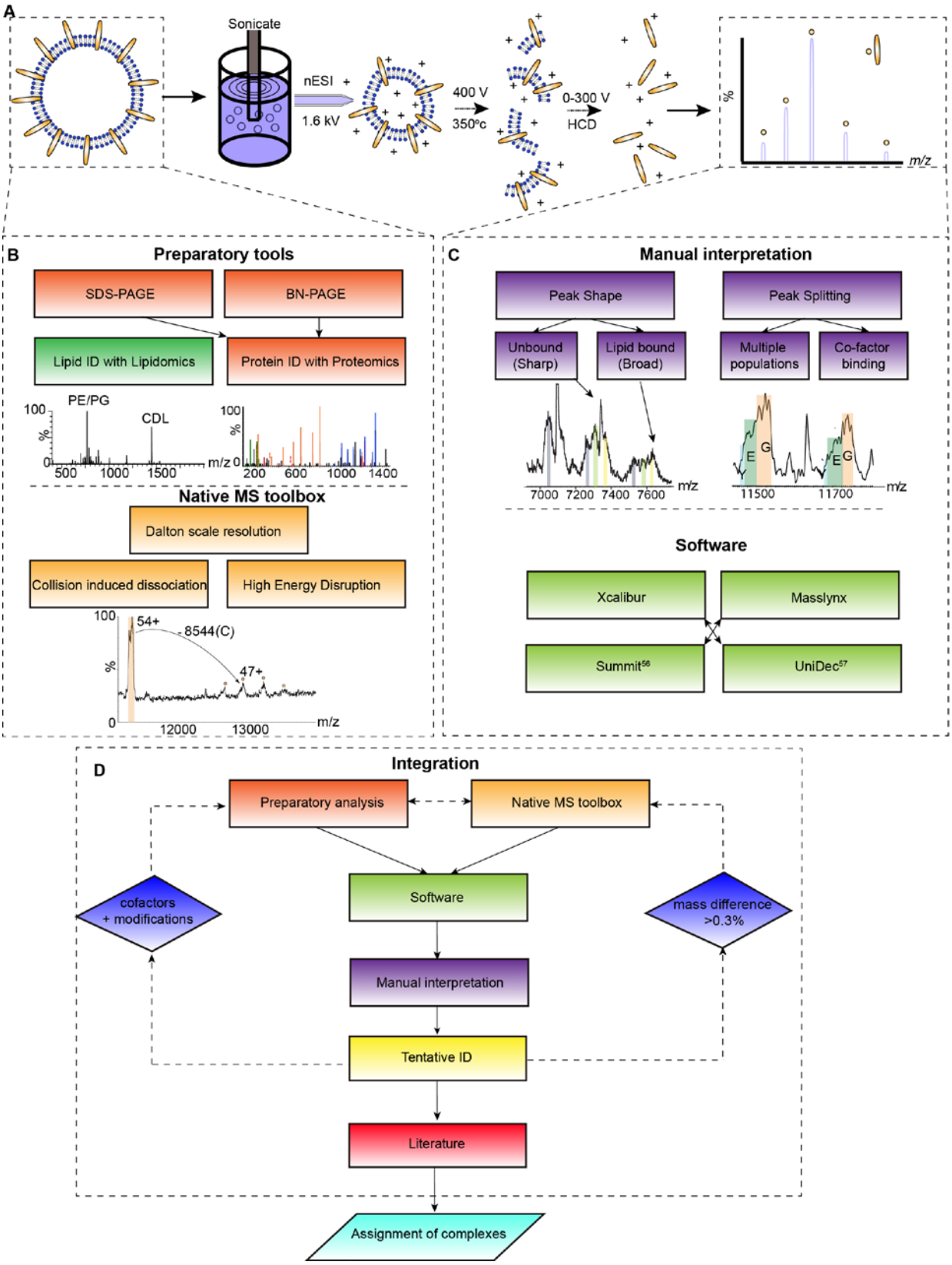
A
Sonicate
nESI
1.6 kV
400 V
350°c
0-300 V
HCD
%
m/z
B
Preparatory tools
SDS-PAGE
BN-PAGE
Lipid ID with Lipidomics
Protein ID with Proteomics
PE/PG
CDL
100
%
0
500
1000
1500
m/z
200
600
1000
1400
Native MS toolbox
Dalton scale resolution
Collision induced dissociation
High Energy Disruption
54+
8544(C)
47+
12000
13000
C
Manual interpretation
Peak Shape
Peak Splitting
Unbound (Sharp)
Lipid bound (Broad)
Multiple populations
Co-factor binding
7000
7200
7400
7600
E
G
11500
11700
Software
Xcalibur
Masslynx
Summit[56]
UniDec[57]
D
Integration
Preparatory analysis
Native MS toolbox
Software
cofactors + modifications
mass difference >0.3%
Manual interpretation
Tentative ID
Literature
Assignment of complexes

**Fig. S2. Procedure for preparation of sonicated lipid vesicles for MS (SOLVE-MS) and flowchart for assignment of complexes.** After vesicles are collected, they are subjected to sonication in 500 mM ammonium acetate within a 50 ml beaker using a probe sonicator and are concentrated in a 4 ml amicon (10-50 kDa molecular weight cut-off) to a volume of approximately 200 µl. Membrane vesicles are then introduced via nano-electrospray into a modified Q-Exactive mass spectrometer, optimised for high electric fields, and are ejected from their membrane environment to yield a mass spectrum of protein ensembles. Two different workstreams are employed to assign protein complexes. In the first standard preparatory tools are employed to identify lipids and proteins (including SDS PAGE gels, blue native gels and standard proteomics analysis of gel bands). For native MS, strategies to disrupt protein complexes are employed including CID and high-energy disruption. In the second stream, peaks in the mass spectrum are first subjected to manual inspection to define peak shape (heterogeneous lipid binding) or peak splitting (cofactor binding). Software tools (*56, 57*) are then employed to further assign peak series and to obtain mass measurements. These work streams are then integrated and a tentative assignment is reached. Extensive literature searching is then employed to query masses against anticipated complexes reported previously. In some cases assignments are rejected as they do not satisfy the stringent mass error limit imposed ± ~ 0.3 %. Differences in established subunit stoichiometry (e.g. ANT1), cofactor binding (cytochrome bd) or interactions between complexes (SecYEG ATPase) are then considered.

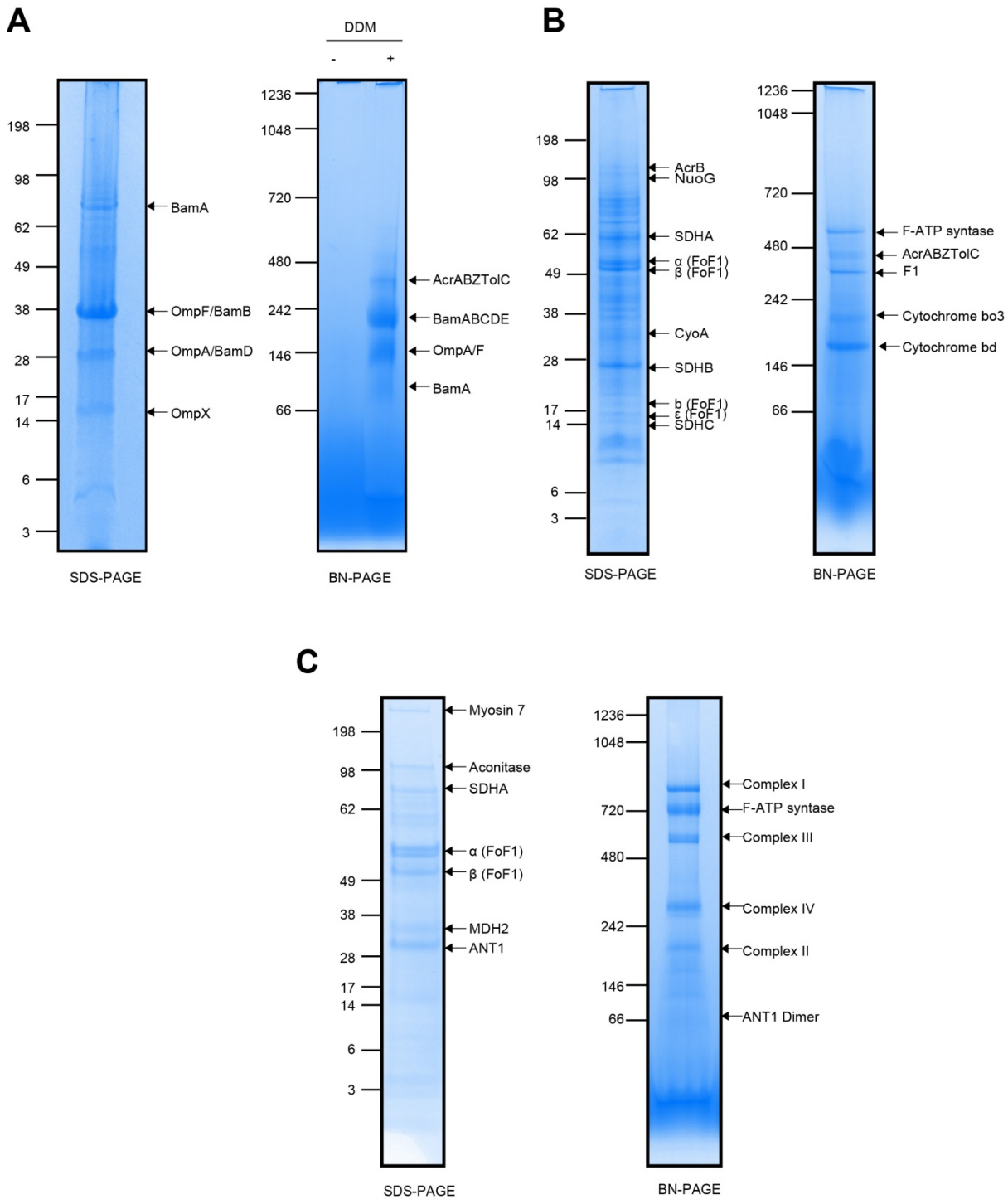


**Fig. S3. Native and denaturing PAGE analysis of whole membrane fractions.** SDS and BN-PAGE analysis of (**A**) *E. coli* outer membranes (**B**) *E. coli* inner membranes and (**C**) Bovine heart mitochondrial inner membranes. For SDS-PAGE analysis, proteins were boiled in sample buffer and run on a 4-12% NuPage bis-tris gel. For native gel analysis, proteins were incubated for 20

mins with 0.5% DDM on ice before being supplemented with native sample buffer and separated on 4-12% Native Page bis-tris gels. Gel kits and running buffers were form Life Technologies.

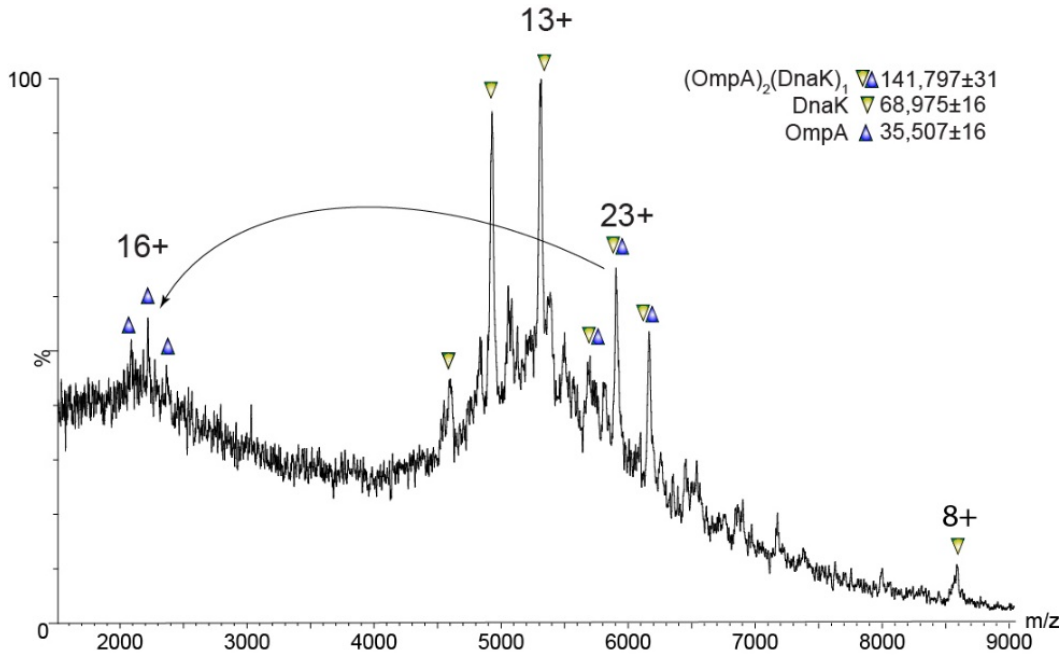


**Fig. S4. High-energy disruption of a 143 kDa complex releases full-length OmpA and DnaK.** Mass spectrum acquired on a Waters Synapt HDMS G1 instrument, with cone, trap and transfer voltages set to 200 V (Total of 600 V). Dissociation of full-length OmpA is achieved by generating an unfolded highly-charged monomer.

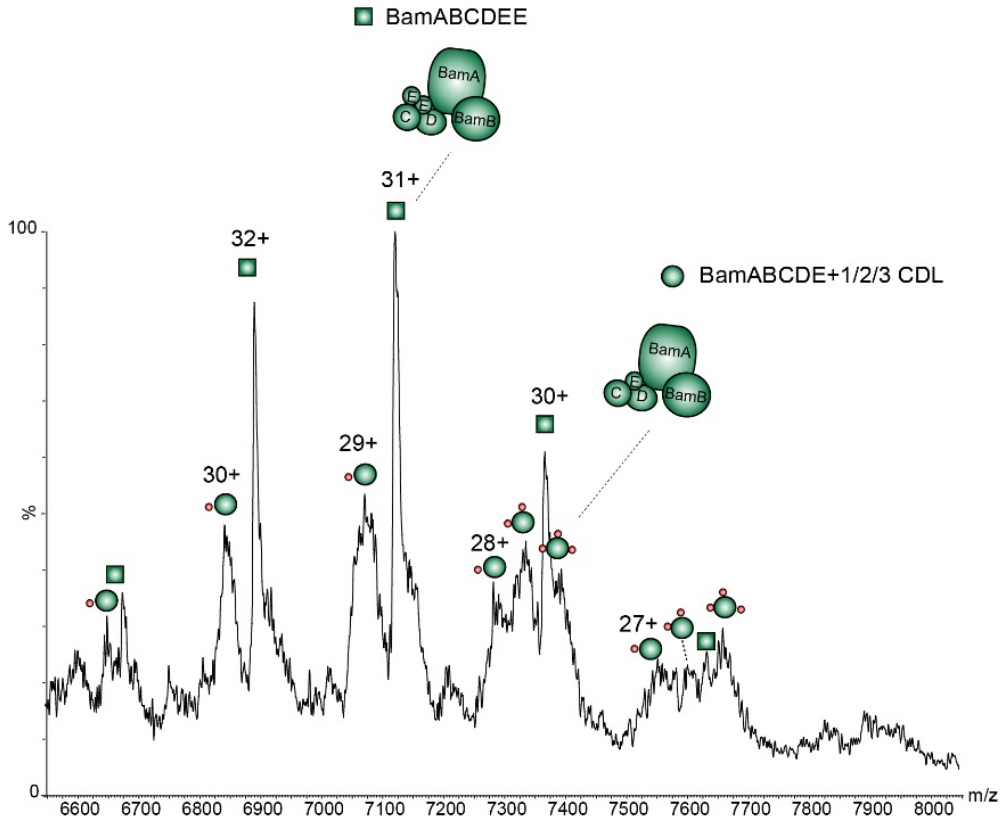


**Fig. S5. BamABCDE can bind up to three cardiolipins.** Expansion of the 6400-8100 m/z region of the spectrum shows a charge state series corresponding to the intact pentameric Bam complex with associated cardiolipins. Low charge states (28+) reveal additional peaks corresponding to binding of up to three cardiolipins. CDL average mass was 1492.9 Da indicative of CDL 76:14.

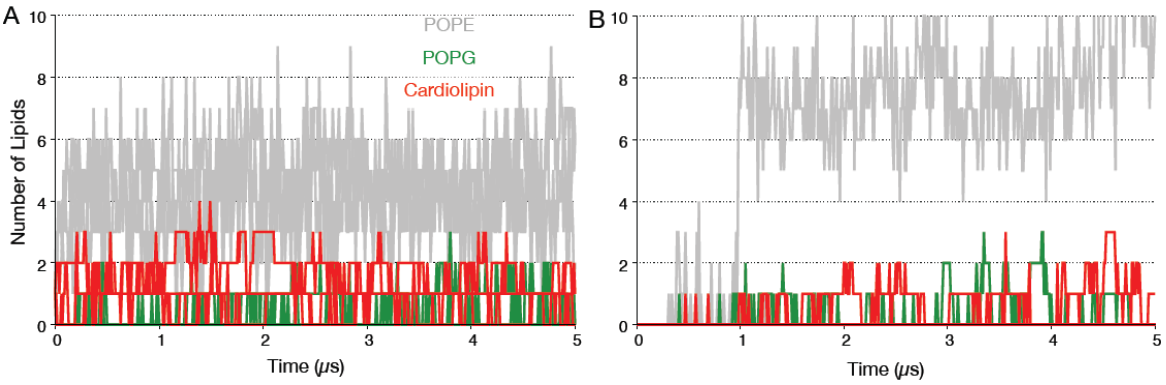


**Fig. S6. Molecular dynamics simulations suggest that BamE within the Bam complex is capable of binding up to three CDL.** The Bam complex was simulated at 323 K for 5 µs. CDL was randomly distributed within the membrane to avoid bias. POPE is labelled in grey, POPG in green and CDL in red. A contact is defined as being within 6 Å. **A** A single subunit of BamE within the complex is capable of binding a maximum of three CDL throughout the simulation and is preferred over POPG. **B** BamE dimers within the complex do not make stable lipid binding interactions.

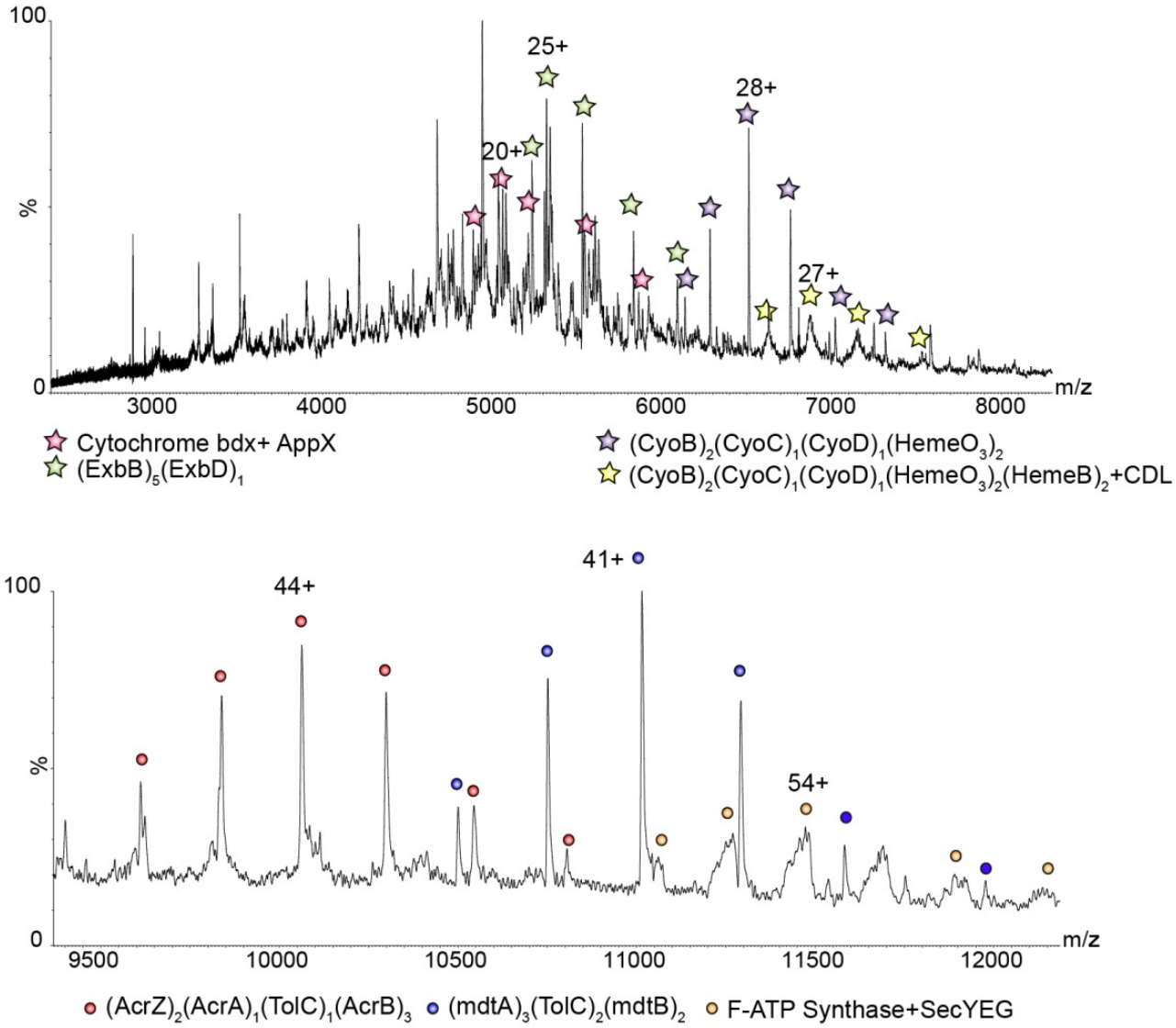


**Fig. S7. Full spectra recorded for *E. coli* inner membrane proteins.** Two cytochromes *bo*$_3$ and bdx, as well as the TonB complex (ExbB/D), are preserved in part (upper spectrum) and subcomplexes of two efflux pumps and the ATP synthase bound to SecYEG are observed (lower spectrum).

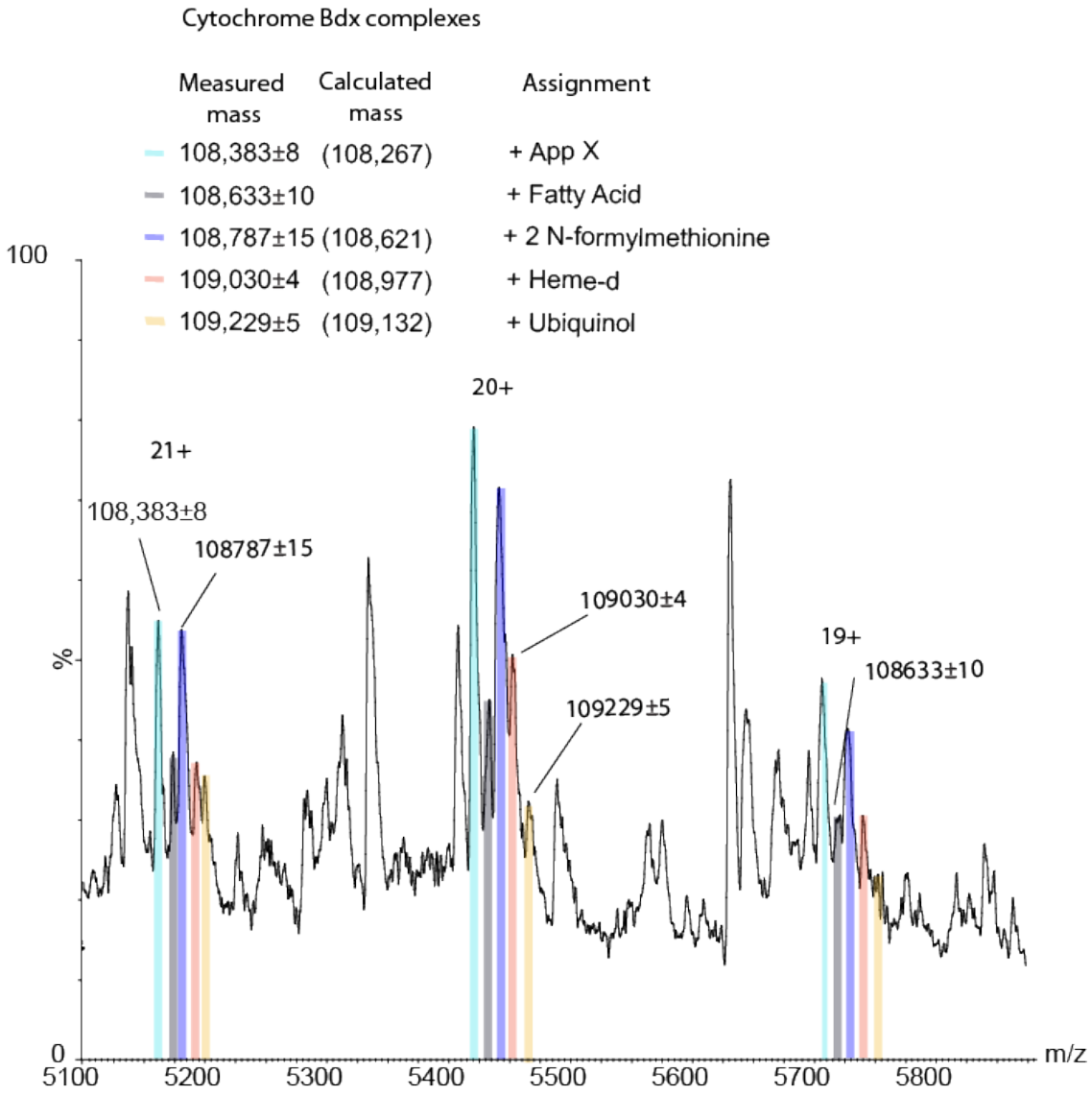


**Fig. S8. Native MS reveals co-factor and AppX binding to Cytochrome bdx.** Expansion of the 5,100-5,900 m/z range shows extensive peak splitting whereby the complex Cytochrome bdx is associated with AppX (aqua) and bound to an unknown small molecule (grey ~250 Da) likely to be a fatty acid. The complex is also modified with 2 N-formylmethionines (blue) and bound either to heme-d (pink) or ubiquinol (orange). Calculated masses are in brackets and peaks are color-coded according to their assignment.

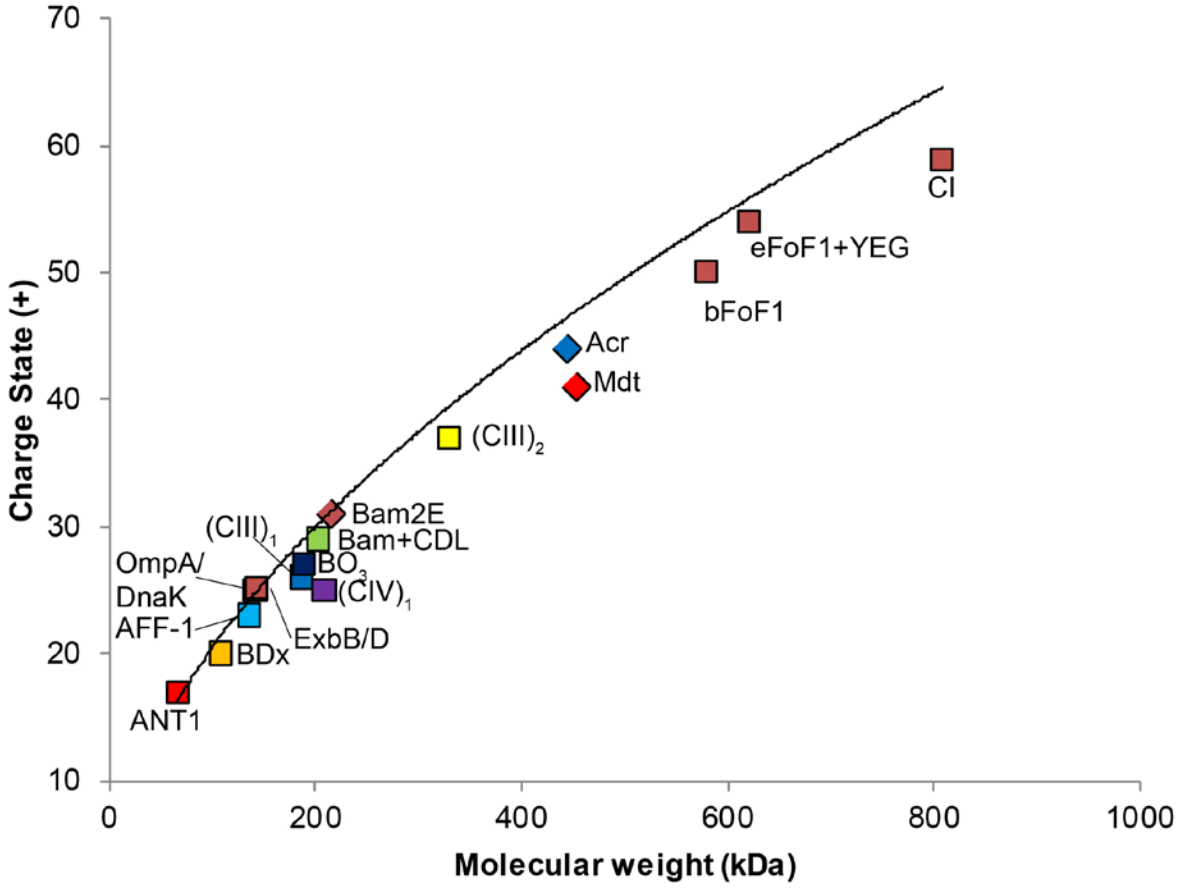


**Fig. S9. Average charge state plotted against the molecular mass of the membrane protein complex is indicative of established membrane protein charge reduction.** The different complexes assigned in this work, were plotted with their molecular mass against their observed average charge state. Expected charge states were calculated using the following equation- $z=1.638xM^{0.5497}$ (black line). The average charge states of most membrane protein complexes are beneath the line, as observed previously for membrane proteins released from detergent micelles (*58*). The position of Mdt implies that it has undergone further gas phase dissociation than Acr for example.

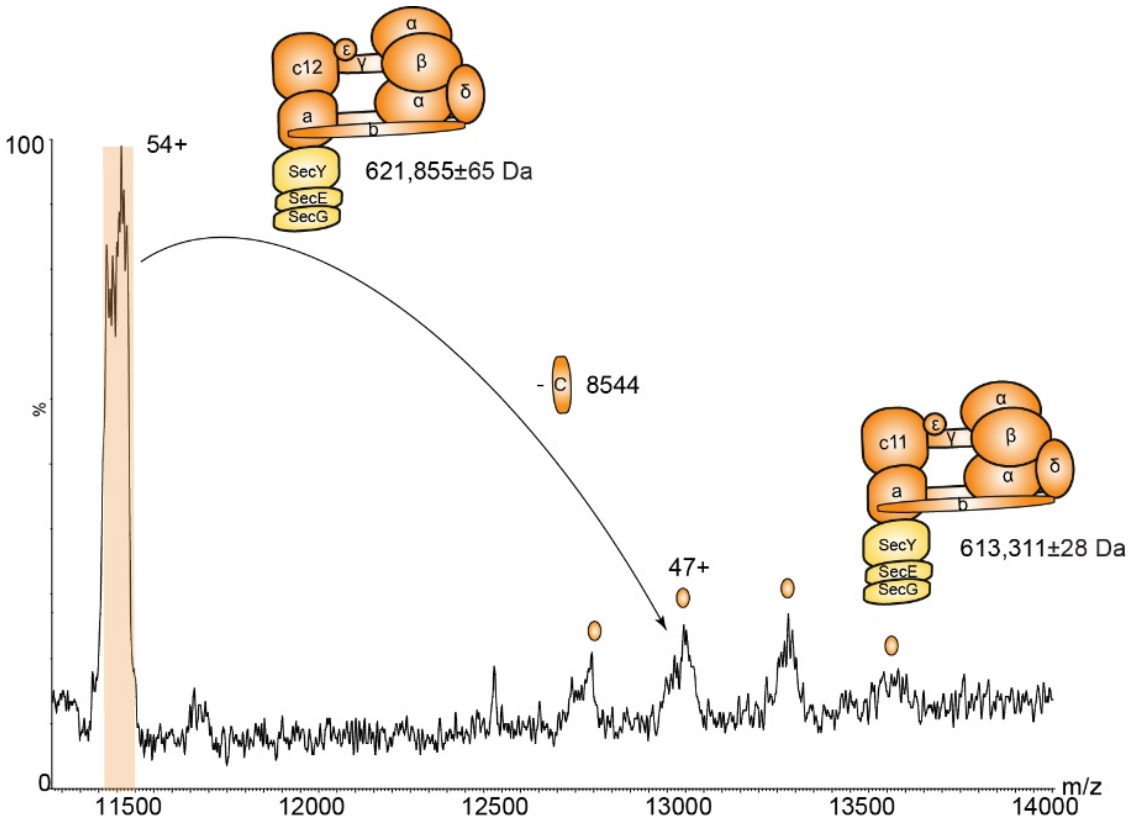


**Fig. S10. Collision induced dissociation of *E. coli* $F_OF_1$ ATP synthase ejects the membrane embedded subunit c.** m/z 11,515 was isolated using the quadrupole with a 100 Da window and the HCD collision energy was increased to 300 V giving a total of 700 V. The stripped complex is consistent with dissociation of a c-subunit and is in contrast to spectra recorded for rotary ATPases released from detergent micelles, in which peripheral subunits are lost preferentially (*59*).

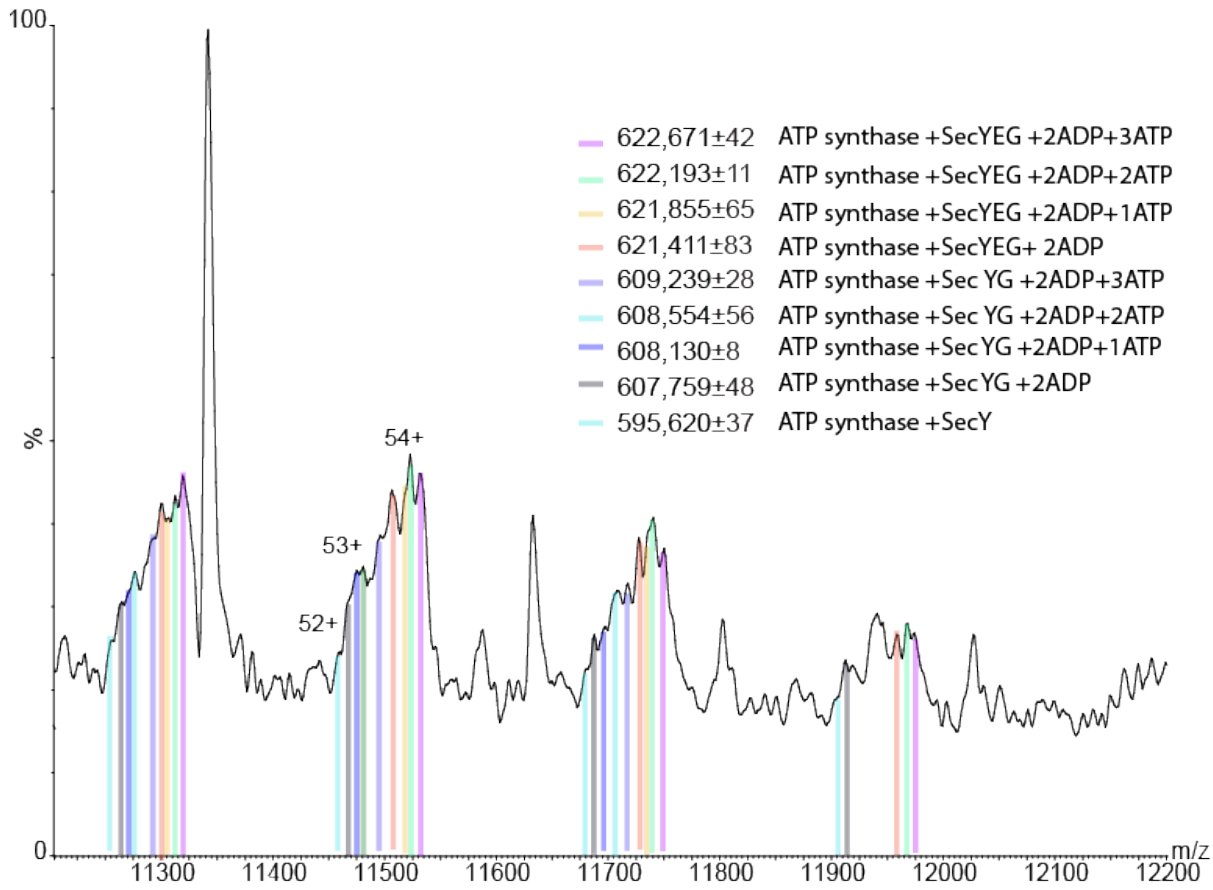


**Fig. S11. High-resolution mass spectrometry of the *E. coli* $FoF_1$ ATP synthase reveals molecular details of interactions.** Expansion of 11,200-12,200 m/z region shows extensive peak splitting. Three major populations are observed and assigned to SecY-bound ATP synthase with a additional populatiosn bound to SecG and SecE with 1-3 additional nucleotides, and a third population containing all SecYEG components bound to the ATP synthase, with a total of 5 bound nucleotide at the highest observable mass. In brackets is the expected mass.

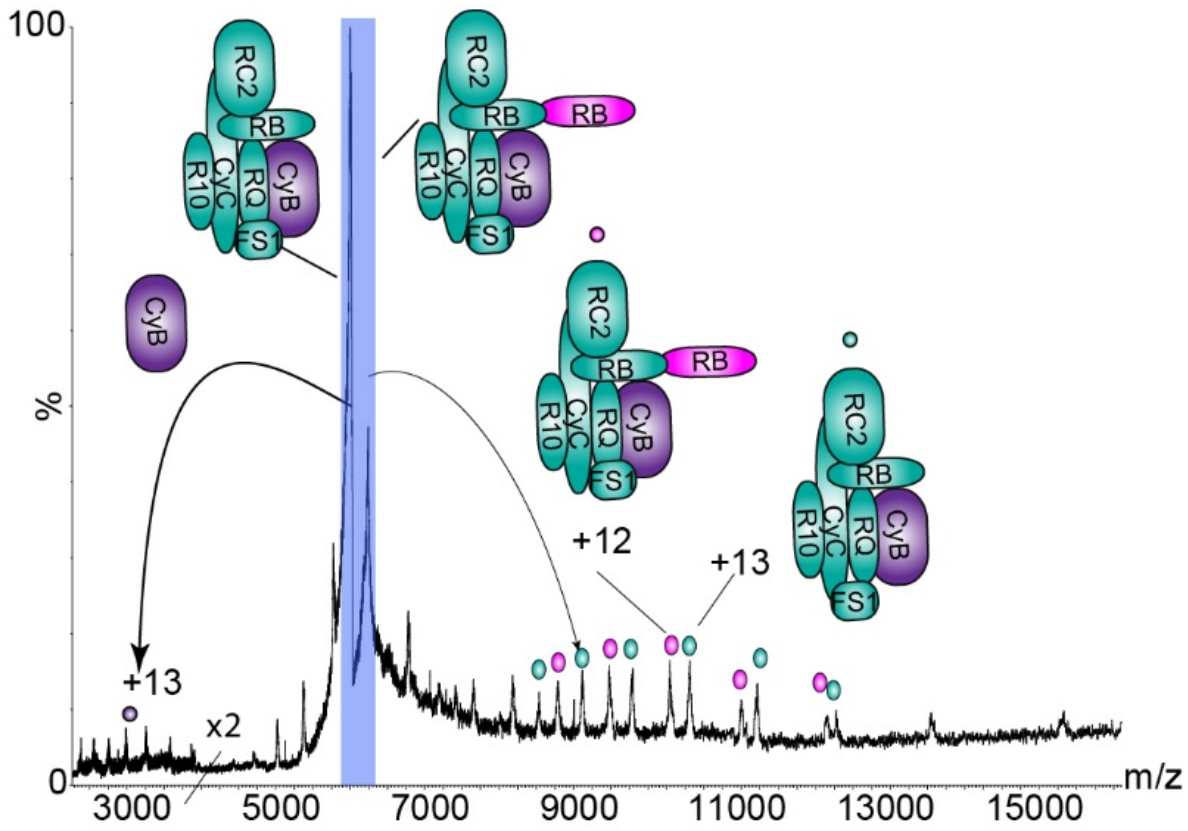


**Fig. S12. CID of two complexes that overlap in the mass spectra mitochondrial inner membranes from *Bos taurus* confirms that they are derived from Complex III.** An unfolded dissociation product Cytochrome B (42.5 kDa) is detected at low m/z (intensity multiplied by a factor of 2) and stripped complexes differing by 13 kDa, observed at high m/z, correspond to the mass of UQUCRB confirming that both these products are derived from Complex III assemblies.

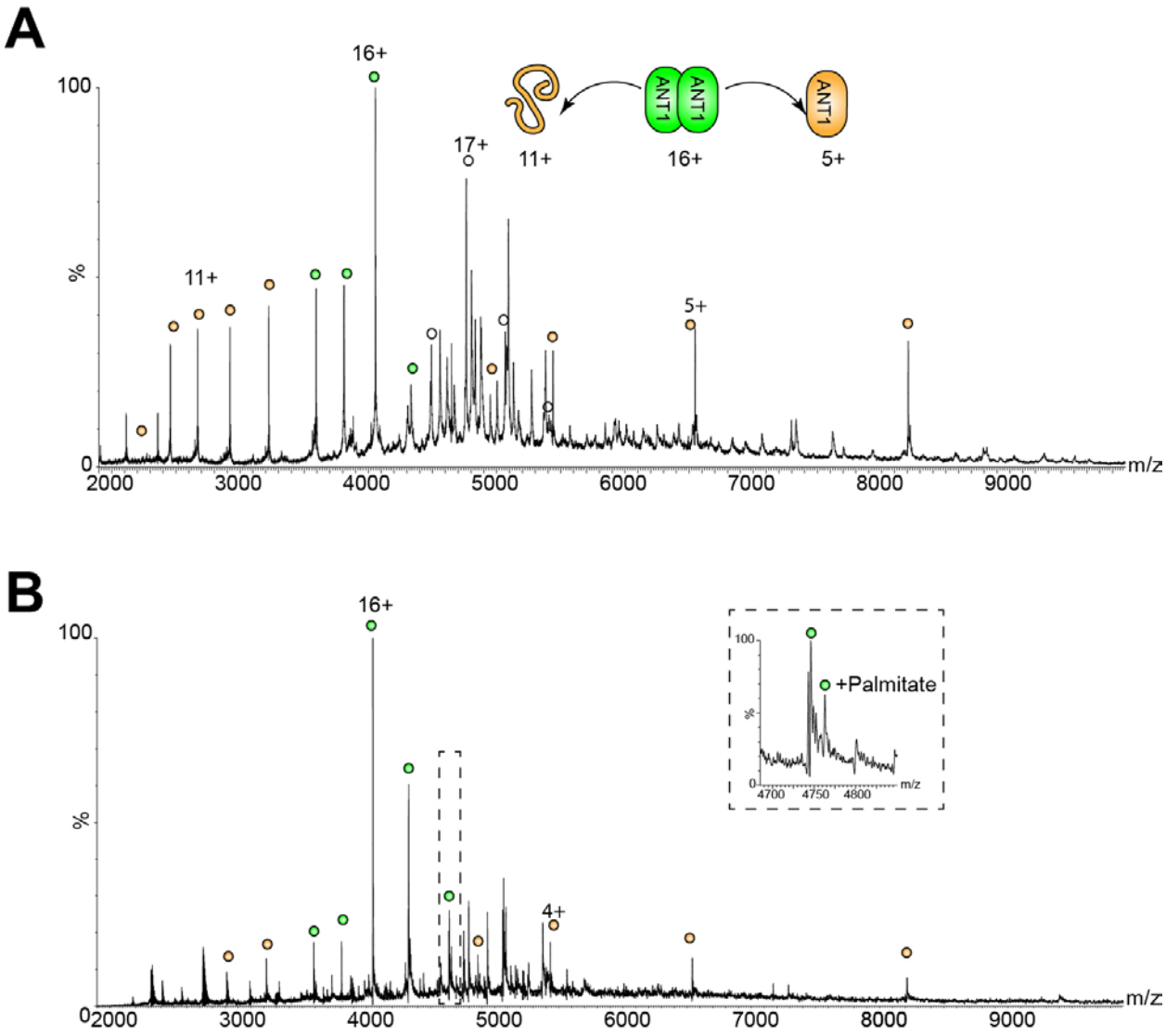


**Fig. S13. ANT1 is predominantly dimeric when ejected directly from bovine mitochondrial membranes.** Mass spectra recorded at 600 V from sonicated, inverted, separated inner membranes (A) and sonicated unseparated non-inverted bovine inner and outer membranes (B) show ANT1 is dimeric in both membranes and that Palmitate is bound to charge states assigned to the dimer in both cases. Inset expansion of the 14+ charge-state of unseparated non-inverted membranes.

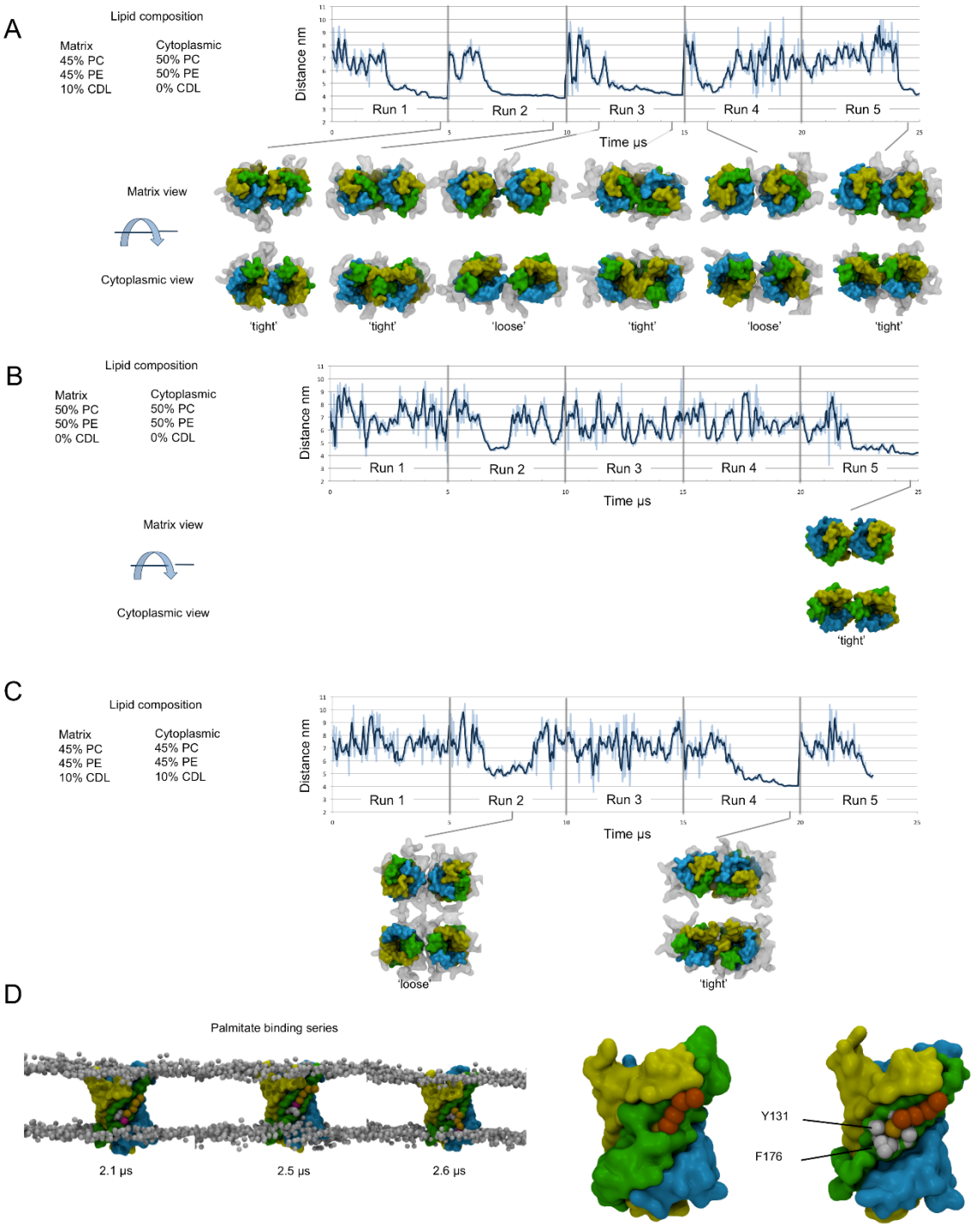


**Fig. S14. Molecular dynamics simulations of ANT1 in model mitochondrial inner membranes. A-C** Modulation of ANT1 dimer formation by the leaflet distribution of CDL. Three membrane compositions were tested in which CDL was present in the matrix leaflet **A**, no leaflets

**B** and both leaflets **C** of the membrane as indicated. The distance between each monomer over time for 5 independent 5 μs trajectories is shown. The 5 trajectories were concatenated for analysis. Snapshots of dimers formed corresponding to the timepoints as indicated are shown from both the cytoplasmic and matrix views. The protein is shown as a surface and coloured according to the pseudo repeats (repeat 1 yellow, repeat 2 is green and repeat 3 cyan). CDL within 1 nm of the protein is shown as a transparent grey surface. A dimer is considered 'tight' when both the matrix and cytoplasmic sides of ANT1 are in close contact. **D** Binding of palmitate to ANT1. The longest residence time observed for palmitate during a single simulation (coloured orange) was 0.4 μs in which the charged headgroup (coloured magenta) buries between helices 3 and 4, sitting above residues Y131 and F176 (grey spheres). The positions of lipid headgroup particles are shown as grey spheres.

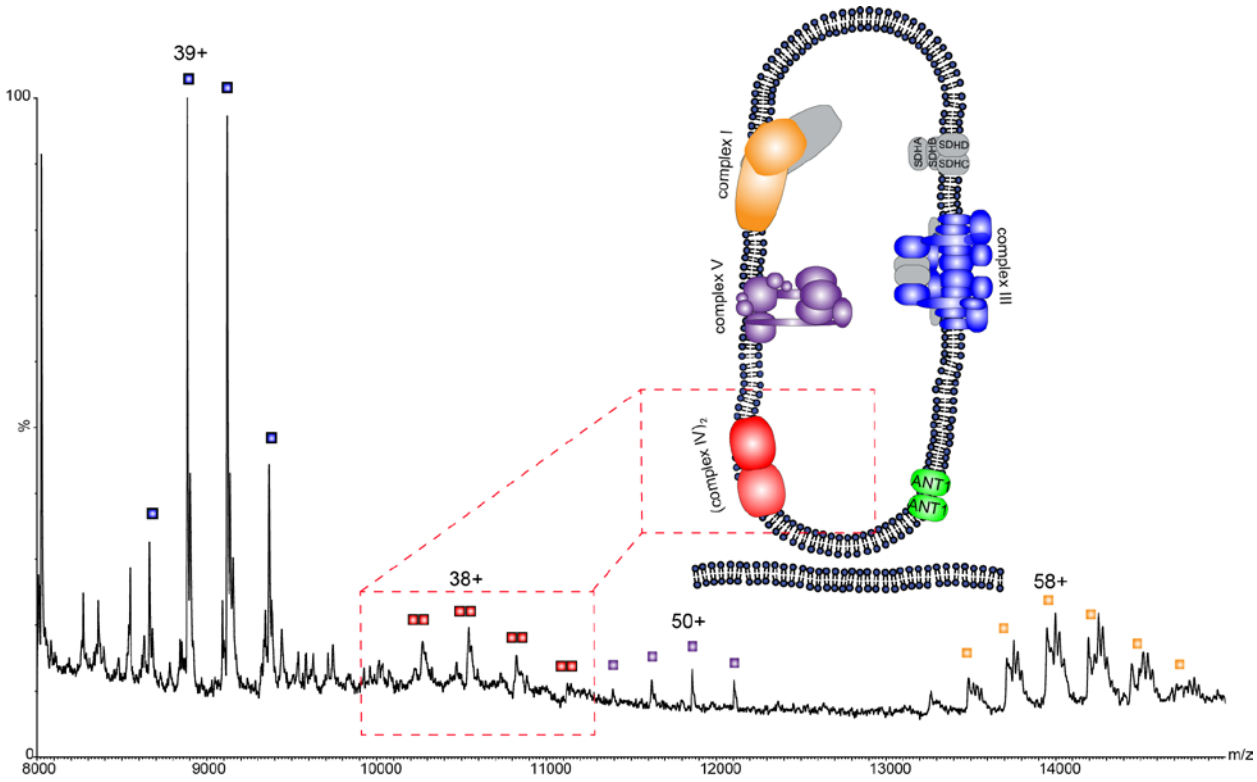


**Fig. S15. Quadrupole isolation of the 8,000-15,000 m/z range confirms the existence of a CIV dimer.** To enhance the details in the higher m/z region of the spectrum, the quadrupole window was reduced from 1,000-20,000 m/z to 8000-15,000 thereby allowing observation of a protein complex with a mass twice that of a CIV monomer assigned as a CIV dimer with associated lipids.

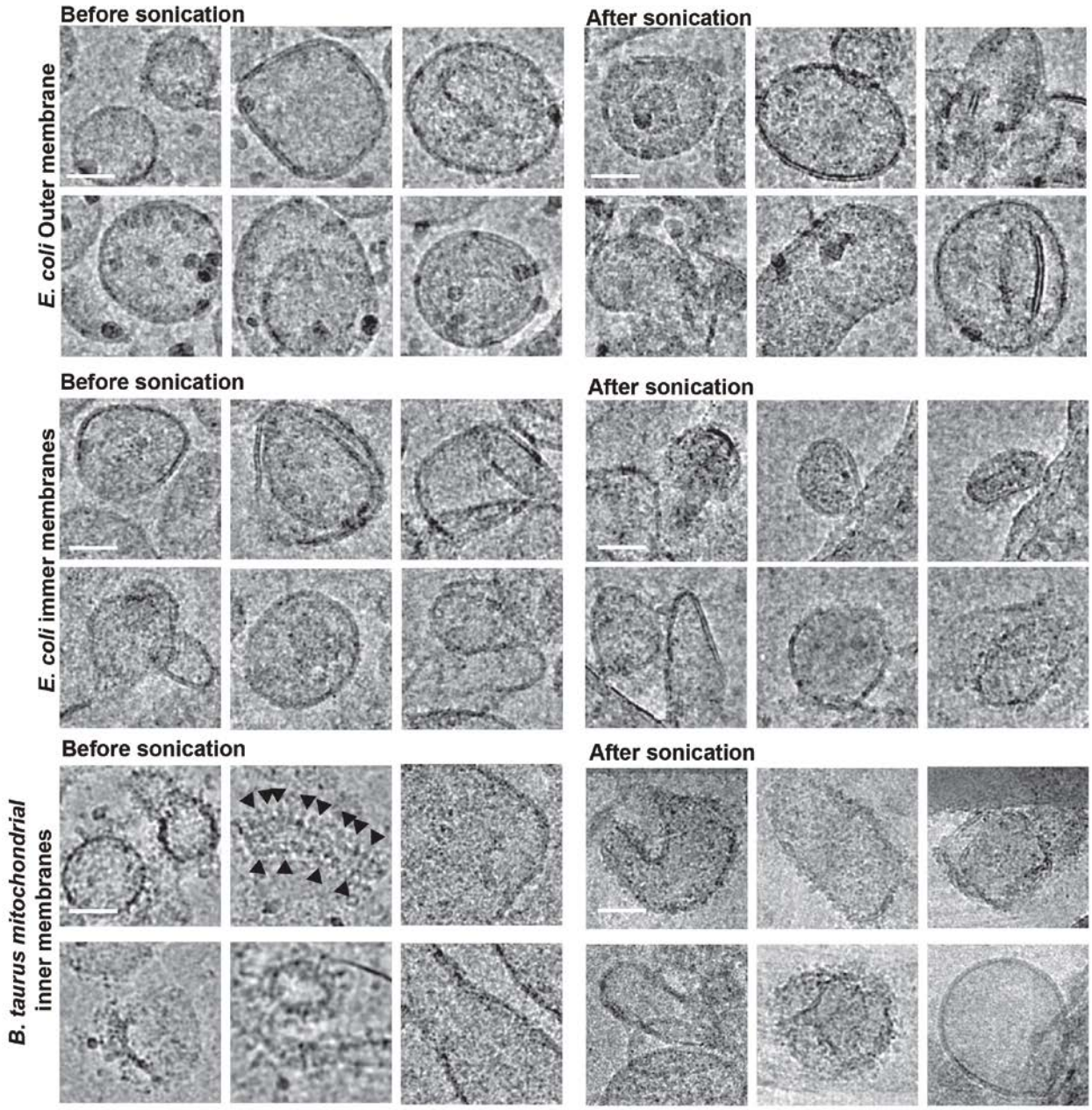


**Fig. S16. Electron Cryo-microscopy of vesicles before and after sonication.** Inner and outer *E. coli* membranes and *B. taurus* mitochondrial membranes were sonicated and visualized by EM. For inner and outer *E. coli* membranes proteins can be seen on the inside and outside of the vesicles. *B. taurus* are inverted as the F1 heads of the ATP synthase (marked with black arrows) can be seen pointing outwards. Scale bar is 50 nm.

**Movie S1.** Movie showing palmitate binding (from Fig 3C) to ANT-1. In this case a palmitate molecule freely diffuses within the matrix leaflet of the membrane before finding the binding site between helices 3 and 4 of ANT-1 where it remains bound for ~0.5 μs before being released again into the membrane. The protein is coloured as in Fig 3C, as a surface with sidechains removed for clarity for pseudo-repeat R2 (green). Tyr132 and Phe177 are shown as yellow spheres. Lipid phosphate groups within 3 nm of the protein are shown as grey spheres. The bound palmitate is coloured magenta (head group) and orange (tail).

**Table S1. Masses and identities of proteins and protein complexes from the outer membrane of *E. coli*.**

| Subunit/Complex<br>OmpA:proOmpA+DnaK | Expected mass (Da) | Measured mass (Da) | Mass difference (Da) | Mass difference (%) |
|---|---|---|---|---|
| DnaK | 69,115 | 69,148±55 | 33 | 0.047 |
| OmpA | 35,172 | | | |
| Pro OmpA | 37,201 | | | |
| DnaK:proOmpA:OmpA (+ADP) | 141,948 | 141,797±31 | -151 | 0.10 |
| Subunit/Complex<br>Bam complex | Expected mass (Da) | Measured mass (Da) | Mass difference | |
| BamA | 88,426* | | | |
| BamB | 40,643*<br>40,663* | | | |
| BamC | 35,163*<br>35,183* | | | |
| BamD | 26,583*<br>26,603 * | | | |
| BamE | 12,383*<br>11,268 (-tag)<br>12,413*<br>11,298 (-tag) | | | |
| BamABCDE+CDL | 203,218*-Light<br>202,103 (-tag)<br>203,288*-Heavy<br>202,179 (-tag) | 203,848±19 (1492 cdl) | 177 | 0.087 |
| BamABCDEE | 213,471 | 213,549±29 | 78 | 0.036 |

*Expected mass based on measurements reported previously (*17*). Heavy and light represent the masses of subunits bound to fatty acids with different chain lengths.

**Table S2. Masses and identities of inner membrane proteins and protein complexes from *E. coli.***

| Subunit/Complex<br>Mdt efflux pump | Expected mass | Measured mass | Mass difference (Da) | Mass difference (%) |
|---|---|---|---|---|
| MdtA | 42,178 | | | |
| MdtB | 112,078 | | | |
| MdtC | 111,010 | | | |
| TolC | 51,454 | | | |
| 3xMdtA 2xMdtB 2xTolC | 453,598 | 453,646±7 | 48 | 0.01 |
| Subunit/Complex<br>Acr efflux pump | Expected mass | Measured mass | Mass difference (Da) | Mass difference (%) |
| AcrA | 113,574 | | | |
| AcrB | 42,197 | | | |
| TolC (outer membrane) | 51,454 | | | |
| AcrZ | 5,300 | | | |
| 2xAcrZ 1xAcrA 1xTolC 3xAcrB | 444,973 | 444,922±6 | 51 | 0.011 |
| Subunit/Complex<br>TonB complex | Expected mass | Measured mass | Mass difference | |
| ExbA (TonB) | 26,094 | | | |
| ExbB | 26,287 | | | |
| ExbD | 15,227 | | | |
| 5xExbB 1xExbD | 146,662 | 146,333±28 | 329 | 0.2 |
| Subunit/Complex<br>ATP-synthase/SecYEG | Expected mass | Measured mass | Mass difference | |
| α | 55,222 | | | |
| β | 50,325 | | | |
| γ | 31,577 | | | |
| δ | 19,332 | | | |
| ε | 15,068 | | | |
| a | 30,303 | | | |
| b | 17,264 | | | |
| c | 8,256<br>N-Formylated- 8,284 | | | |

| | | | | |
|---|---|---|---|---|
| SecY | 48,512 | | | |
| SecE | 13,643 | 13,652 | 9 | 0.065 |
| SecG | 11,365 | | | |
| ATP synthase holo-complex | 546,857 (12c-formyl) | 595-622kDa | | |
| Holocomplex+SecY | 595,369 | 595,620±37 | 251 | 0.042 |
| Holocomplex+SecY+SecG +(2 ADP) | 607,588 | 607,759±48 | 171 | 0.028 |
| Holocomplex+SecYEG | 621,231 | 621,411±83 | 180 | 0.029 |
| Subunit/Complex<br>Cytochrome bd | Expected mass | Measured mass | Mass difference (Da) | Mass difference (%) |
| CydA | 58,205 | | | |
| CydB | 42,423 | | | |
| CydX | 4,042 | | | |
| AppX | 3,597 | | | |
| Heme B558 | 617 | | | |
| Heme B595 | 617 | | | |
| Heme d | 710 | | | |
| Ubiquinol | 865 | | | |
| Cytochrome bdx(+AppX) complex | 108,267 | 108383 ± 8 | 116 | 0.1 |
| Bdx+AptX+2N-formylmethionine | 108,621 | 108,633 ± 10 | 12 | 0.011 |
| Bdx+AptX+Heme d | 108,977 | 109,030 ± 4 | 53 | 0.048 |
| Bdx+AptX+Ubiquinol | 109,132 | 109,229 ± 5 | 97 | 0.088 |
| Subunit/Complex<br>Cytochrome *bo*$_3$ | Expected mass | Measured mass | Mass difference (Da) | Mass difference (%) |
| CyoA | 32,218 | | | |
| CyoB | 74,368 | | | |
| CyoC | 22,623 | | | |
| CyoD | 12,029 | | | |
| HemeO | 838.8 | | | |
| Heme B | 616.487 | | | |
| 2xCyoB 1xCyoC 1xCyoD 2xHemeO3 | 185,064 | 185,096±5 | 32 | 0.017 |
| 2xCyoB 1xCyoC 1xCyoD 2xHemeB 2xHemeO 1xCDL | 187,528 (1.4-1.6 CDL) | 188,103±4 | 575 | 0.311 |

**Table S3. Masses and identities of inner mitochondrial membrane proteins and protein complexes from *Bos taurus.***

| Subunit/Complex<br>ANT1 Dimer | Expected mass (Da) | Measured mass (Da) | Mass difference (Da) | Mass difference (%) |
|---|---|---|---|---|
| ANT1 (+3 Succinilation reported in mouse – uniprot database) | 33,187 | 33,195±11 | 8 | 0 |
| 2xANT1 | 66,374 | 66,387±13 | 13 | 0 |
| Subunit/Complex<br>Aconitase | Expected mass | Measured mass | Mass difference (Da) | Mass difference (%) |
| Aconitase | 82,401 | 82,635±9 | 234 | 0.2 |
| Subunit/Complex<br>Complex III | Expected mass | Measured mass | Mass difference (Da) | Mass difference (%) |
| UQCRC1 | 49,212 | | | |
| UQCRC2 | 46,523 | | | |
| UQCRH | 9,175 | | | |
| UQCRB | 13,345 | | | |
| UQCR10 | 7,326 | | | |
| UQCR11 | 6,520 | | | |
| UQCRQ | 9589 | | | |
| UQCRFS1 | 21,609 | | | |
| UQCRFS1 transit peptide | 7,955 | | | |
| MTCYB | 42,591 | | | |
| CyC1 | 27,987 | | | |
| Complex III (Partial monomer)<br>CyB CyC UQCRC2 UQCRFS1 UQCRB UQCRQ UQCR10 | 168,970 | 168,580±50 | 390 | 0.23 |
| 2xComplex III (Partial monomer) | 337,940 | 338,615±12 | 675<br>heme | 0.199 |
| Subunit/Complex<br>Complex IV | Expected mass (Da) | Measured mass (Da) | Mass difference (Da) | Mass difference (%) |
| Cox1 | 57,032 | | | |
| Cox2 | 26,021 | | | |

| | | | | |
|---|---|---|---|---|
| Cox3 | 29,933 | | | |
| Cox4 Isoform 1 | 17,152 | | | |
| Cox5A | 12,433 | | | |
| Cox5B | 10,670 | | | |
| Cox6A1 | 9,538 | | | |
| Cox6B1 | 10,025 | | | |
| Cox6C | 8,478 | | | |
| Cox7A2 | 6,609 | | | |
| Cox7B | 6,357 | | | |
| Cox7C | 5,441 | | | |
| Cox8B | 4,961 | | | |
| Heme a | 853 | | | |
| Heme a3 | 859 | | | |
| Cardiolipin (CDL)* | 1448 | | | |
| Phosphatydilethanolamine (PE)* | 760 | | | |
| Complex IV monomer | 208,299 | 208,191±55 | 108 | 0.04 |
| Subunit/Complex<br>Complex V | Expected mass (Da) | Measured mass (Da) | Mass difference (Da) | Mass difference (%) |
| α** | 55,263 | 55,271±0.5 | 8 | 0.0144 |
| β** | 51,563 | 51,754±0.5 | 191 | 0.3 |
| γ** | 30,256 | 30,143±4 | 113 | 0.3 |
| δ** | 15,065 | 15,064±2 | 1 | 0.066 |
| ε** | 5,793 | 5,652±1 | 141 | 2.4 |
| a** | 24,788 | 24,813±4 | 25 | 0.1 |
| b** | 24,669 | 24,691±1 | 22 | 0.089 |
| c** | 7,608 | 7,650±1 | 42 | 0.55 |
| d** | 18,692 | 18,602±3 | 90 | 0.48 |
| e** | 8,321 | 8190±2 | 131 | 1.5 |
| f** | 10,297 | 10,206±2 | 91 | 0.8 |
| g** | 11,417 | 11,326±2 | 91 | 0.7 |
| A6L** | 7,973 | 7,963±1 | 10 | 0.1 |
| F6** | 8,958 | 8,957±2 | 1 | 0.01 |

| | | | | |
|---|---|---|---|---|
| 6.8PL** | 6,834 | 6,834±1 | 0 | 0 |
| DAPIT** | 6,453 | 6,303±1 | 150 | 2.32 |
| OSCP** | 20,930 | 20,929±4 | 1 | 0.004 |
| Holocomplex (8 c, 3 α, 3 β, 1copy of all the rest) | 581,948 | 581,046±62 | 902 | 0.15 |
| Subunit/Complex<br>Complex I | Expected mass (Da) | Measured mass (Da) | Mass difference (Da) | Mass difference (%) |
| NDUFS7 | 20,077 | | | |
| NDUFS8 | 20,195 | | | |
| NDUFV2 | 23,814 | | | |
| NDUFS3 | 26,413 | 26,612 | | |
| NDUFS2 | 49,146 | | | |
| NDUFV1 | 48,499 | | | |
| NDUFS1 | 76,960 | | | |
| NU1M | 35,670 | | | |
| NU2M | 39,254 | | | |
| NU3M | 13,054 | | | |
| NU4M | 52,099 | | | |
| NU4LM | 10,797 | | | |
| NU5M | 68,286 | | | |
| NU6M | 19,078 | | | |
| NDUFS6 | 10,535 | | | |
| NDUFA12 | 17,090 | | | |
| NDUFS4 | 15,337 | | | |
| NDUFA9 | 39,115 | | | |
| NDUFAB1 | 10,109 | | | |
| NDUFA2 | 10,948 | | | |
| NDUFA1 | 8,105 | | | |
| NDUFB3 | 11,009 | | | |
| NDUFA5 | 13,184 | | | |
| NDUFA6 | 14,922 | | | |
| NDUFA11 | 14,626 | | | |
| NDUFB11 | 2,325 | | | |
| NDUFS5 | 12,536 | | | |
| NDUFB4 | 15,053 | | | |
| NDUFA13 | 16,542 | | | |
| NDUFB7 | 16,266 | | | |
| NDUFA8 | 19,959 | | | |
| NDUFB9 | 21,657 | | | |

| | | | | |
|---|---|---|---|---|
| NDUFB10 | 20,956 | | | |
| NDUFB8 | 2,537 | | | |
| NDUFC2 | 14,096 | | | |
| NDUFB2 | 8,493 | | | |
| NDUFA7 | 12,545 | | | |
| NDUFA8 | 9,217 | | | |
| NDUFA4 | 9,324 | | | |
| NDUFB5 | 16,726 | | | |
| NDUFB1 | 6,966 | | | |
| NDUFC1 | 5,828 | | | |
| NDUFA10 | 36,692 | | | |
| NDUFA4L2 | 9,984 | | | |
| NDUFV3 | 8,437 | | | |
| BDUFB6 | 15,392 | | | |
| Complex I ΔNDUFV1 ΔNDUFS1 ΔNDUFA6 (42/45 subunit, each present in one copy) | 809,202 | 809,101±57 | 101 | 0.012 |
| Complex I ΔNDUFV1 ΔNDUFS1 ΔNDUFA6 ΔNDUFS3 (41/45 subunits) | 782,789 | 782478±27 | 311 | 0.039 |

*Lipid identities from (*42*).

**Subunit masses measured by a monolithic column construct.

***Measurement from native MS.


41. L. A. Baker *et al.*, Magic-angle-spinning solid-state NMR of membrane proteins. *Methods Enzymol* **557**, 307-328 (2015).
42. S. Yoshikawa, K. Muramoto, K. Shinzawa-Itoh, M. Mochizuki, Structural studies on bovine heart cytochrome c oxidase. *Biochim Biophys Acta* **1817**, 579-589 (2012).
43. R. J. Rose, E. Damoc, E. Denisov, A. Makarov, A. J. Heck, High-sensitivity Orbitrap mass analysis of intact macromolecular assemblies. *Nat Methods* **9**, 1084-1086 (2012).
44. J. Gault *et al.*, High-resolution mass spectrometry of small molecules bound to membrane proteins. *Nat Methods* **13**, 333-336 (2016).
45. S. S. Bird, V. R. Marur, M. J. Sniatynski, H. K. Greenberg, B. S. Kristal, Lipidomics profiling by high-resolution LC-MS and high-energy collisional dissociation fragmentation: focus on characterization of mitochondrial cardiolipins and monolysocardiolipins. *Analytical chemistry* **83**, 940-949 (2011).
46. C. Bechara *et al.*, A subset of annular lipids is linked to the flippase activity of an ABC transporter. *Nat Chem* **7**, 255-262 (2015).
47. A. Shevchenko, H. Tomas, J. Havlis, J. V. Olsen, M. Mann, In-gel digestion for mass spectrometric characterization of proteins and proteomes. *Nat Protoc* **1**, 2856-2860 (2006).
48. D. N. Mastronarde, Automated electron microscope tomography using robust prediction of specimen movements. *J Struct Biol* **152**, 36-51 (2005).

49. P. C. Hsu *et al.*, CHARMM-GUI Martini Maker for modeling and simulation of complex bacterial membranes with lipopolysaccharides. *J Comput Chem* **38**, 2354-2363 (2017).
50. K. H. Kim *et al.*, Structural characterization of Escherichia coli BamE, a lipoprotein component of the beta-barrel assembly machinery complex. *Biochemistry* **50**, 1081-1090 (2011).
51. S. K. Fegan, M. Thachuk, Suitability of the MARTINI Force Field for Use with Gas-Phase Protein Complexes. *J Chem Theory Comput* **8**, 1304-1313 (2012).
52. G. Bussi, D. Donadio, M. Parrinello, Canonical sampling through velocity rescaling. *J Chem Phys* **126**, 014101 (2007).
53. M. Parinello, A. Rahman, Polymorphic transitions in single crystals: A new molecular dynamics method. *J Appl Phys* **52**, 7182-7190 (1981).
54. B. Hess, C. Kutzner, D. van der Spoel, E. Lindahl, GROMACS 4: Algorithms for Highly Efficient, Load-Balanced, and Scalable Molecular Simulation. *J Chem Theory Comput* **4**, 435-447 (2008).
55. W. Humphrey, A. Dalke, K. Schulten, VMD: visual molecular dynamics. *J Mol Graph* **14**, 33-38, 27-38 (1996).
56. T. Taverner *et al.*, Subunit architecture of intact protein complexes from mass spectrometry and homology modeling. *Accounts of chemical research* **41**, 617-627 (2008).
57. M. T. Marty *et al.*, Bayesian deconvolution of mass and ion mobility spectra: from binary interactions to polydisperse ensembles. *Analytical chemistry* **87**, 4370-4376 (2015).
58. N. Morgner, F. Montenegro, N. P. Barrera, C. V. Robinson, Mass spectrometry--from peripheral proteins to membrane motors. *J Mol Biol* **423**, 1-13 (2012).
59. M. Zhou *et al.*, Mass spectrometry of intact V-type ATPases reveals bound lipids and the effects of nucleotide binding. *Science* **334**, 380-385 (2011).